

An experimental and numerical approach for optimization of internal and external corrugations with various geometries in cylindrical thin-walled concertina energy absorbers under quasi-static axial load

Reza Rahpeima, Iman Nateghi Boroujeni & Ali Alavi Nia

To cite this article: Reza Rahpeima, Iman Nateghi Boroujeni & Ali Alavi Nia (2023): An experimental and numerical approach for optimization of internal and external corrugations with various geometries in cylindrical thin-walled concertina energy absorbers under quasi-static axial load, *Mechanics of Advanced Materials and Structures*, DOI: [10.1080/15376494.2023.2235357](https://doi.org/10.1080/15376494.2023.2235357)

To link to this article: <https://doi.org/10.1080/15376494.2023.2235357>



Published online: 31 Jul 2023.



Submit your article to this journal 



Article views: 21



View related articles 



View Crossmark data 

An experimental and numerical approach for optimization of internal and external corrugations with various geometries in cylindrical thin-walled concertina energy absorbers under quasi-static axial load

Reza Rahpeima^{a*}, Iman Nateghi Boroujeni^{b*†}, and Ali Alavi Nia^c

^aGraduate institute of biomedical electronics and bioinformatics, College of Electrical Engineering and Computer Science, National Taiwan University, Taipei, Taiwan; ^bDepartment of Mechanical Engineering, Tarbiat Modares University, Tehran, Iran; ^cDepartment of Mechanical Engineering, Bu-Ali Sina University, Hamedan, Iran

ABSTRACT

Thin-walled tubes have been extensively used as energy absorbers in many engineering structures that are under dynamic or quasi-static loads. In this article, the effect of corrugation and its geometry on the collapse characteristics of aluminum concertina tubes under quasi-static axial load is investigated both experimentally and numerically. The numerical simulations were performed with the use of LS-Dyna commercial software. Then, several chosen samples were tested experimentally to verify the results of the simulation. Forty different samples with four different corrugation geometries including singly isosceles triangular corrugation, continual isosceles triangular corrugation, continual scalene triangular corrugation, and continual semi-circular corrugation, and each with 10 different size dimensions were simulated. Among all of these simulations, six of them, each with two replicates were subjected to experimental tests. Experimental examples are aluminum cylindrical thin-walled tubes with the same thickness, height, and diameter that corrugations with different geometries are applied to them by the use of the cold rolling method. Finally, to describe the findings in more theoretical terms, a comparison between our obtained results and earlier theoretical investigations is made. The results show a significant influence of corrugations application on the improvement of the collapse characteristics of the cylindrical tubes so that the collapse style of intact tubes can be controlled by applying corrugations. The results show that by increasing the amplitude and number of corrugations, the absorbed energy, and the initial maximum force decrease. It is also found that among the different corrugation geometries, the corrugations with singly isosceles triangular geometry have the highest energy absorption as well as the lowest initial maximum force.

ARTICLE HISTORY

Received 5 March 2023

Accepted 5 July 2023

KEYWORDS

Energy absorber; peripheral corrugations; concertina thin-walled structures; axial loading; quasi-static load

1. Introduction

In many engineering structures that are under dynamic or quasi-static load, thin-walled energy absorbers are used to eliminate or reduce the damage to the structure. The ratio of strength to weight and the amount of energy absorption of thin-walled metal structures are sufficient. The behavior of thin-walled metal structures under compressive axial load as energy absorbers has been studied for many years. These structures are buckled under the axial load and dampen the kinetic energy of the structure by doing plastic work. The collapse process of thin-walled structures has great importance and so far, many researchers have investigated this issue. The most common type of absorbers is cylindrical thin-walled shells that absorb energy by collapsing under axial load. Axial buckling as one of the best methods of energy absorption is performed in three concertina, diamond, and Euler buckling modes. In each of these modes, if the length of all the absorbers is assumed to be the same, the concertina buckling mode has the highest

energy absorption, which is due to the more deformation of the pipe walls in the concertina mode [1].

When a thin-walled tube is compressed along the axis, successive local wrinkles are formed along the tube wall. The compressive force-displacement graph can be plotted for the collapse of these structures. The bounded surface between the curve and the displacement axis represents the amount of energy absorbed by the absorber the more it is, the better. Also, the maximum force for the collapse to begin (initial maximum force) is another important characteristic of the energy absorber. The lower this quantity, the more desirable the absorber will be. Besides, the collapsing force of these cylindrical tubes fluctuates substantially as wrinkles form. This fluctuation reduces the energy absorption of the tube and is a negative consequence of energy absorbers [1]. So, several studies aim to improve these fluctuations and stability of the collapse process, increase the energy absorption capacity, and reduce the initial maximum force which is reviewed below.

CONTACT Reza Rahpeima  rahpeima.reza@gmail.com  College of Electrical Engineering and Computer Science, National Taiwan University, Taipei, Taiwan.

*These authors contributed equally to this work.

†Department of Mechanical Engineering at Bu-Ali Sina University, Hamedan, Iran.

© 2023 Taylor & Francis Group, LLC

In 1983, Abramowicz performed several quasi-static and dynamic axial compressive tests on a series of thin-walled steel tubes with circular and square sections. He presented the important concept of effective crushing distance [2]. In 1986, Abramowicz *et al.* proposed the equation of wrinkle length for symmetrical states. This equation is in good agreement with the results of experimental tests [3, 4]. In 1994, Langseth *et al.* investigated the effect of pre-buckling of tubes on reducing initial maximum force [5]. In 1999, Lee *et al.* investigated the effect of triggering and impact-induced deformation on the energy absorption capacity of aluminum tubes under quasi-static pressure. Their study showed that the triggering reduces the initial maximum collapsing force [6]. In 2005, El-Hage *et al.* performed a numerical study on the effect of applying various types of deformation on tubes including edge chamfering, applying geometrical defects, and any dependent combination of them. This study showed that the initial deformation of the tube can significantly control the initial maximum force [7]. Cylindrical or square tubes that are filled with foam and are under axial load have been studied by many researchers. Wierzbicki and Abramowicz [1], Reid *et al.* [8], and Reddy and Wall [9] are some of them. In 2010, Alavi-Nia *et al.* after studying the energy absorption capacity of absorbers with different cross sections (circular, rectangular, hexagonal, and triangular), concluded that the absorbers with circular cross sections have the highest energy absorption capacity [10]. In 2010, Bi *et al.* performed an investigation on the modeling and optimization of foam-filled thin-walled columns for crashworthiness designs [11]. In 2016, Progressive collapse analysis and energy absorption of carbon-epoxy composite tubes under axial impact load were tested by Luo *et al.* [12]. In 2016, Alavi-nia *et al.* investigated aluminum structures with three cylindrical nested concentric tubes under quasi-static load. Their results showed that these structures while having a small initial force, could have greater energy absorption capacity than conventional single tubes [13]. In 2021, the microstructure of the cross section of bamboo served as the inspiration for Yang *et al.*'s (MTTN) multicellular thin-walled tube with N-equilateral triangles. The sensitivity study for the geometric parameters of MTT24, which demonstrated the greatest crashing performance among MTTNs with $N \leq 30$, was undertaken after an investigation of the crashworthiness of MTTNs under axial impact [14]. In 2022, Zhang *et al.* designed and studied the crushing properties of a collection of bionic thin-walled tubes that were inspired by the microstructure of bamboo and beetle forewings. The finite element model of bionic thin-walled tubes underwent experimental verification as well [15]. In 2023, Zhang *et al.* performed a numerical investigation on the axial crushing damage of hybrid thin-walled aluminum/CFRP (carbon fiber reinforced polymer) tubes. Due to its advantageous weight-saving and crashworthiness, metal/CFRP hybrid constructions have been used extensively in the automobile industry. Their work establishes a nonlinear finite element (FE) model to investigate the axial crushing behavior of thin-walled aluminum/CFRP tube constructions [16]. Due to the

lightweight nature and material efficiency of thin-walled structures, they could have the potential for sustainable construction practices. In 2023, Olutola *et al.* reviewed applications of thin-walled structures in sustainable construction practices. By conducting a comprehensive literature review, they investigated the current state of knowledge, identifies key challenges, and proposes effective decision-making strategies for sustainable design and construction of thin-walled structures [17]. Ma *et al.* (2022) also provide a review of the geometric design, deformation mode and mechanism, and energy absorption of the patterned thin-walled structures in the form of tubes, fold cores, and metamaterials [18].

Applying peripheral grooves that are repeatedly cut on the inner or outer surface of the tube at specified intervals was introduced by Daneshi and Hosseiniour as an effective solution to improve the crashworthiness characteristics of thin-walled tubes [19]. In 2014, Rezvani and Damghani Nouri proposed an analytical model for axisymmetric axial crushing of thin-walled frusta tubes containing annular grooves [20]. In 2018, Asanjarani *et al.* studied the crush force efficiency, specific energy absorption, energy absorption per crush length, and maximum and average crush forces of straight and grooved tapered thin-walled tubes with a variety of cross-section shapes (circle, ellipse, square, rectangle, hexagon, and octagon). They discovered that by making cost-effective geometry alterations, the behavior of these structures may be improved against dynamic axial and oblique impact stress [21]. Also, in 2019, Alavi-Nia *et al.*, evaluate the effect of inner and outer transverse and longitudinal grooves on energy absorption characteristics of cylindrical thin-walled tubes under quasi-static load. Also, in 2021, Xie *et al.* studied the crashworthiness of circular tubes subjected to radial extrusion under quasi-static loading. The deformation behavior and force response of these tubes were investigated by experiment and FEA methods [22].

Applying corrugation to improve crashworthiness characteristics is another method that recently has received a lot of attention. In 2012, Eyyazian *et al.* investigated the energy absorption characteristics of corrugated tubes with different geometries under lateral loading. It has been observed that corrugated tubes absorb four times as much energy as intact tubes with the same dimensions and weight [23]. They also experimented on corrugated aluminum tubes under quasi-static axial loading. These experiments showed that the introduction of corrugations can significantly improve the energy absorption properties of metal tubes [24]. In 2017, Rawat *et al.* investigated the collapse behavior and energy absorption in elliptical tubes with functionally graded corrugations [25]. In 2018, Abolfathi and Nia optimized the energy absorption properties of thin-walled tubes with combined deformation of folding and circumferential expansion under axial load [26]. In 2018, San Ha *et al.* by mimicking the coconut tree configuration, applied corrugations on thin-walled tubes to increase their energy absorption, reduce the initial force, and stabilize the collapse process. They investigated the effect of wavelength and angle of wavelet on energy absorption and collapse mode and finally presented a theoretical model to predict the mean collapse force of these

tubes under dynamic load [27]. In 2019, Sadighi *et al.* investigated a novel axially half-corrugated thin-walled tube for energy absorption under axial loading [28]. In 2019, a crashworthiness experimental analysis of a novel aluminum bi-tubular corrugated tube is performed by Eyyazian *et al.* [29]. In 2020, Ma *et al.* performed a crashworthiness analysis of thin-walled bio-inspired multicell corrugated tubes under quasi-static axial loading [30]. In 2020, Li *et al.* investigated the crashworthiness of multicell circumferentially corrugated square tubes (CCSTs) with cosine and triangular configurations. The crashworthiness of several multicell CCSTs was investigated under multiple loading angles. The results showed that the cosine and triangular multicell CCSTs with crisscross ribs exhibited the best performance [31]. Also, in 2020, Li *et al.* investigated the crashworthiness performance of corrugation-reinforced multicell tubular structures. They proposed a structural design method combining multicell and multicorrugation to improve the crashworthiness of tubes [32]. In 2021, Yang *et al.* studied the crashworthiness of hierarchical truncated conical shells with corrugated cores. They proposed hierarchical truncated conical shells (HTCS) with corrugated cores as a novel energy absorber [33]. In 2021, based on machine learning, Li *et al.* predicted and improved the energy absorption of corrugation-reinforced multicell square tubes. In their research, an energy-absorbing tube that combines multicorner and multicell designs was created. Because machine learning can handle both numerical and categorical answers, it was used to forecast and optimize the proposed tube's crashworthiness. Their findings demonstrated that as the studied geometric parameters increased, so did the specific energy absorption, the peak crushing force, and the propensity of the unstable deformation mode to manifest [34].

As aforementioned, researchers have different methods of controlling the collapse mechanism including heat treatment, filling the tube with foam, creating grooves, creating corrugations, changing the location of load applying, and so forth. The effect of all of these different methods on the crashworthiness of energy absorbers was investigated. However, this field needs further study. The higher the uniformity of the force in the force-displacement graph, the better the absorber. Applying corrugation along the tube length has a great impact on the uniformity of the force-displacement graph. It is necessary to conduct a systematic study on the influence of different corrugation geometry to gain a broad understanding of the properties of the collapse of circular tubes with alternating corrugations. Some researchers have investigated the effect of corrugation, but what is lacking is to optimize different waveforms and dimensions to reach the most efficient corrugation geometry and dimension. In this research, to derive comparative advantages and differentiate between different types of corrugations and to achieve their effects on energy absorption characteristics, several corrugations with different geometries will be comprehensively investigated (numerically, experimentally, and theoretically). numerical and experimental results will be obtained and will be compared with the theoretical formulas available.

2. Materials and methods

This chapter is broken down into four subsections. In each subsection, different considerations along with different steps for gathering the necessary information for both numerical and experimental procedures are elaborated.

2.1. Corrugation's geometry

In this article, aluminum cylindrical tubes with a height of 120 mm, an outer diameter of 70 mm, and a thickness of 2 mm are selected. Since compressive buckling is an important response mode of corrugated thin-walled tubes. According to the investigation done by Andrews *et al.* [35], the height-to-diameter and thickness-to-diameter ratio of the considered tube is selected in such a way that the structure is stable against global buckling in compressive loads, and its failure mode is a concertina, which absorbs the most energy. Different samples have different types of corrugations. These corrugations have different types of geometry, different wavelength, and different amplitude. As shown in Figure 1, four different types of geometry along with the intact tube are considered as follows:

1. Intact Tube (IT)
2. Singly Isosceles Triangular Corrugation (SIsoT)
3. Continual Isosceles Triangular Corrugation (CIsoT)
4. Continual Scalene Triangular Corrugation (CsT)
5. Continual Semi-Circular Corrugation (CsC)

In this figure, d is the wavelength of the corrugation. For each of these corrugation geometry types, 10 different cases which have different corrugation dimensions (different wavelengths or amplitudes) are considered. These 10 different cases are numbered from 1 to 10 and their dimensional characteristics are mentioned in Table 1. These case numbers are added to the end of each sample's name to indicate the corrugation dimension. For instance, the CIsoT2 sample is a tube with Continual Isosceles Triangular corrugation that has dimensional characteristics of case number 2 (shown in Table 1). In Table 1, d and a are the wavelength and amplitude of the corrugations, respectively. The values set for d and a are selected after the initial simulations. For a better understanding, the corrugation geometry of CsC6 and CsC10 samples are illustrated with details in Figure 2.

2.2. Cold rolling process

Cold roll forming was used to create the corrugations on the wall of the tubes. For this purpose, hard steel rollers with different surface profiles were used for each of the samples. Figure 3 shows some of the rollers used. The mentioned rollers are mounted on two parallel rotary axes according to Figure 4. These axes gradually close together to form the intended corrugations on the tube wall.

Among all of the simulation samples, IT, CIsoT6, CIsoT1, CsC1, CsT1, and SIsoT4 were made for experimental tests to validate the simulation results. The samples made

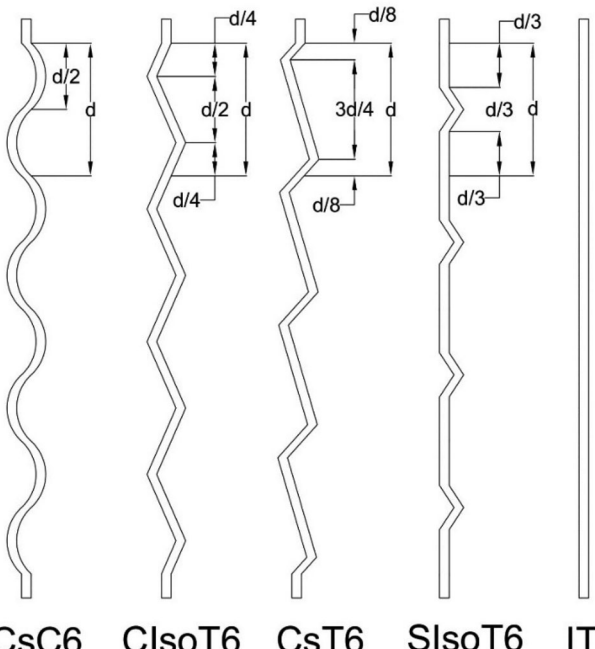


Figure 1. Different types of corrugation geometries.

Table 1. Dimensional case numbers of different samples.

	$a = 2$ (mm)	$a = 3$ (mm)	$a = 5$ (mm)
$d = 12.2$ (mm)	1	2	–
$d = 18.4$ (mm)	3	4	–
$d = 27.5$ (mm)	5	6	7
$d = 36.6$ (mm)	8	9	10

are shown in Figure 5. Two duplicates were prepared for each of the above samples and their test results are averaged and mentioned in the next sections.

2.3. Tension test

Before the main tests, two tension samples were prepared according to the ASTM-E8-E9 standard to obtain the stress-strain curve and mechanical properties of aluminum [36]. The wire-cut tension samples were placed under axial tension by STM-150 apparatus (STM-150 Cap.150 kN) at a velocity of 5 mm/min and the stress-strain diagram was extracted. The tension samples along with the STM-150 apparatus are shown in Figure 6.

The stress-strain curve obtained from the experiment is “engineering” and for use in software, it must be converted to the “true” curve (shown in Figure 7). So, Eqs. (1) and (2) are used to convert the engineering stress-strain curve to the true one. In these equations, e , s , ε , and σ are engineering strain, engineering stress, real strain, and real stress, respectively.

$$\varepsilon = \ln(1 + e) \quad (1)$$

$$\sigma = s(1 + e) \quad (2)$$

2.4. Numerical methodology and grid generation

In this article, numerical simulations were performed using LS-Dyna software for the quasi-static loading, two upper

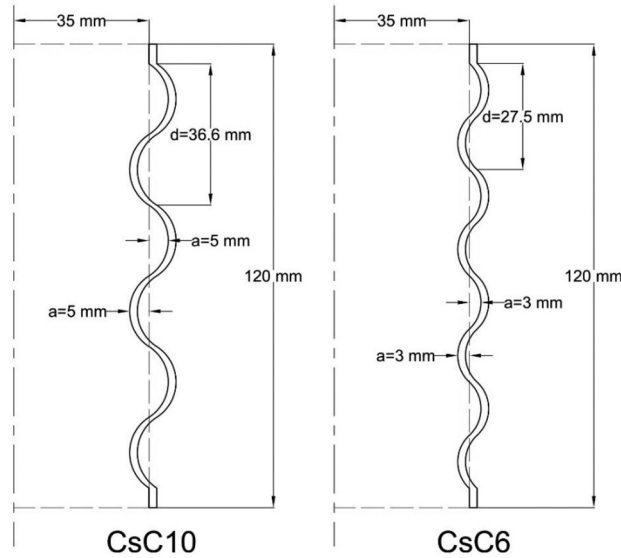


Figure 2. Corrugation geometry of CsC group; (a) CsC6, (b) CsC10.

and lower rigid jaws are used at two ends of the cylindrical tube. The lower jaw is stationary and the upper jaw is moved 85 mm downward with a constant speed in a quasi-static manner. All of the elements are selected as “solid” and the tube material model is considered “Mat-PIECEWISE_LINEAR_PLASTICITY.” This material model fits well with the actual behavior of aluminum. The stress-strain curve given to the software is the true stress-strain curve displayed in Figure 7. The contact between jaws and tube is considered as “Automatic_Surface_to_Surface” contact and the contact of different parts of the tube with each other is considered to be “Automatic_Single_Surface.” According to the mentioned stress-strain curve and the mechanical properties handbooks, Poisson’s coefficient, the elastic modulus, and the yield stress of aluminum are considered 0.3, 60 GPa, and 65 MPa, respectively. The coefficients of static and dynamic friction between the tube and jaws are considered 0.33 and 0.31, respectively, and between the parts of tubes with each other considered 0.17 and 0.15, respectively.

For the grid generation, several simulations with different mesh dimensions were carried out and the absorbed energy is calculated for each of them. When the finer grids do not change the numerical results, the most refined grid is considered to achieve an appropriate grid independency level. The Mesh convergence diagram is shown in Figure 8. So, according to this diagram, the optimum mesh element is considered to be a square cube with a side length of about 1 mm. For a better understanding, the optimum grid generated for the CIsoT6 sample is shown in Figure 9 for instance.

3. Results

This section is divided into three sub-sections. First, simulation results are mentioned, then, results obtained from the experimental tests are illustrated. In the third subsection, these results are compared with each other, and validation of simulation results is performed.

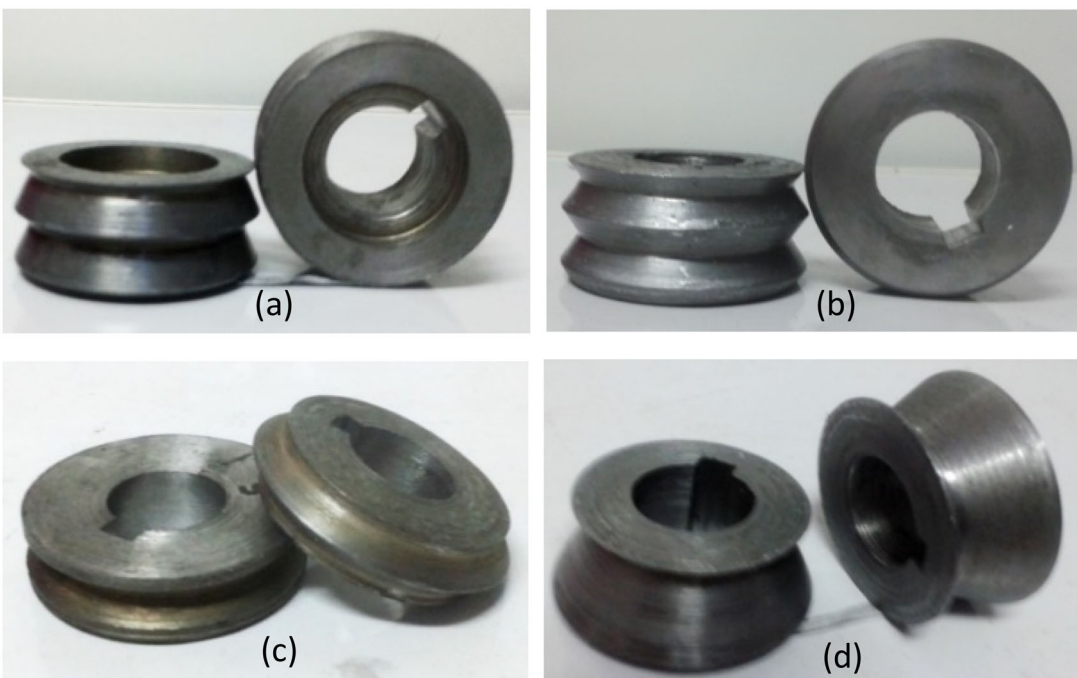


Figure 3. Rollers made for experimental tests; (a) CsT1 sample roller, (b) ClsoT1 sample roller, (c) SIsoT4 sample roller, (d) CsT6 sample roller.



Figure 4. Cold roll forming of tubes for creating the corrugations.

3.1. Simulations

For investigating the effect of corrugation geometry and dimension on the Energy Adsorption Characteristics of Cylindrical Thin-walled tubes, 40 different samples are simulated. The collapse characteristics obtained from numerical simulation results are shown in Table 2. These characteristics include absorbed energy, average collapse force, maximum initial collapse force, collapse style, and specific energy absorbed (SEA).

3.2. Experiments

As aforementioned, some of the simulated samples have been made and tested experimentally to validate and verify the accuracy of the simulations. In experimental samples due to manufacturing constraints, it was not possible to



Figure 5. The formed experiment samples.



Figure 6. STM-150 apparatus (left side) and tension samples (right side).

corrugate all of the 40 simulated samples. So, six of them are considered for experimental tests as a validation of the simulation method. Two duplicates were prepared for each of these six samples and their test results are obtained. These samples were pressed between the jaws of the STM-150 apparatus according to Figure 10.

Figure 11 shows pictures of different stages of the SIsoT4 sample collapse and Figure 12 shows pictures of some of the samples after a complete collapse. Also, the averaged results of each of the two duplicate experimental samples are calculated and mentioned in Table 3.

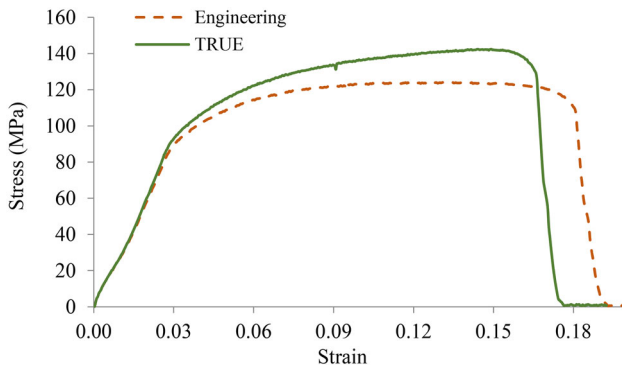


Figure 7. Engineering and true stress–strain curve of the aluminum tension samples.

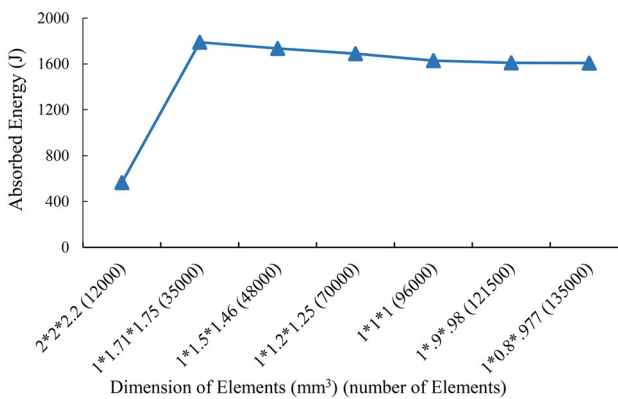


Figure 8. Mesh convergence diagram.

3.3. Results comparison and validation

To validate the simulation results, the results of the experimental tests and simulations are compared and the difference between the experimental results and simulation ones is calculated. This difference between the experiment and simulation results is mentioned in Table 4. Also, In Figure 13, the force–displacement graphs extracted from the simulations along with both of the experiments are illustrated for each of the samples. It should be mentioned that there are a few noises and small fluctuations around the beginning of loading and generally, the beginning of each folding in numerical results, which are negligible.

According to the results, in most cases, experiments with acceptable approximation confirm the results of numerical analysis. The error is due to the heterogeneity and impurity of the aluminum tube material, the way the test tubes are made, and the conditions of the tests. For the forming of the corrugations, rolling rollers were made to the size of just one corrugation and by using this one roller, the desired number of corrugations was formed on the wall of each tube. Therefore, the corrugation distances may not be exactly the same and may cause an error in the results of some samples, especially the sample SIsoT4, which has distant single corrugations. Another drawback to the rolling was the thinning of the tube wall at the antinode of the corrugations due to the rolling process. This phenomenon reduced the strength and resistance of the tubes to buckling, resulting in a difference between the numerical and

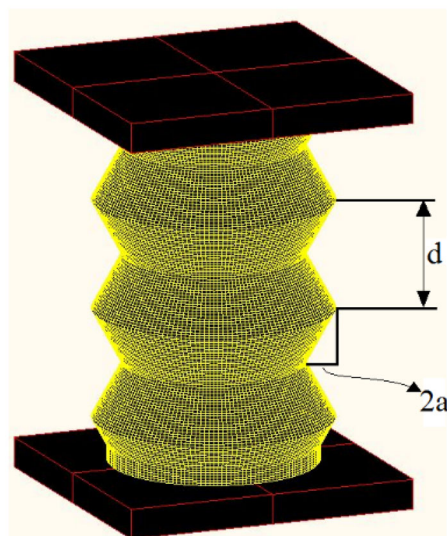


Figure 9. Optimum grid generated for the ClsoT6 sample in LS-Dyna.

experimental results. This is evident perfectly in the CsC1 sample. Also, the incomplete alignment of the tubes between the rolling rollers has resulted in rounding of the antinode points of the corrugations, while in the simulation, the angles in these points are perfectly matched with the geometry of the corrugation mentioned. As a result, the different stress concentration in the simulation and experiment is another factor for the difference in results. During the testing process, another factor that causes this difference between experiment and simulation results is that the top or bottom of the tube may not be perfectly adjacent and aligned with the jaw surface. Resulting in uneven loading that causes faster buckling in some parts, causing asymmetry of conditions and loading. In the end, for a better comparison, samples with 50% collapsing in both the experiment and simulation are shown in Figure 14.

4. Discussion

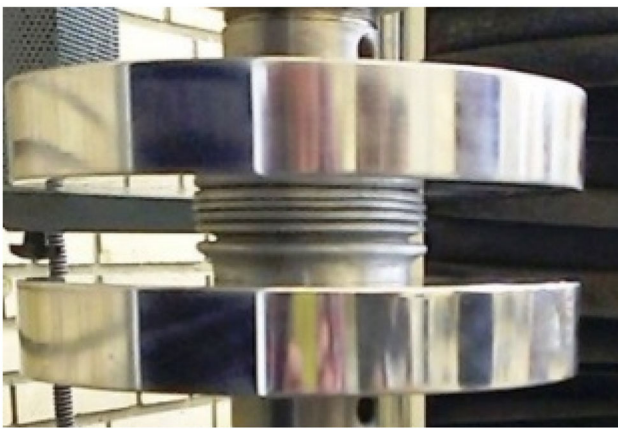
In this section, by comparing simulation results, the effect of different corrugation geometries and dimensions on the collapse characteristics and mechanism of concertina tubes is elaborated in detail. Also, for a better understanding of the physics and laws in principles of structural mechanics, a summary of analytical approaches for various corrugation geometries and the comparison between our results and their prediction is mentioned.

4.1. Effect of the corrugation geometry

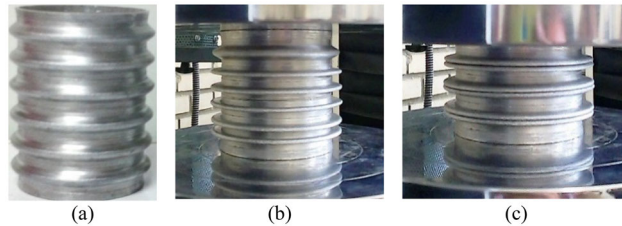
For investigating the effect of just corrugation type on the energy absorption characteristics, results for samples with a state number of 1 (which have corrugations with the same wavelength and amplitude) and IT samples are compared with each other. The amounts of absorbed energy, specific energy, average collapse force, and maximum initial force for both experiment and simulation are shown in Figure 15. It should be mentioned that the SIsoT1 sample has not been

Table 2. Collapse results of the simulated samples.

Samples name	Absorbed energy (kJ)	Average force (kN)	Maximum initial force (kN)	Collapse style	Crushing length (%)	Specific energy (kJ/kg)
IT	1.6078	18.92	38.6	Axisymmetric	70	14.23
ClsoT1	1.03	12.14	12	Axisymmetric	70	9.12
ClsoT2	0.52	6.11	5.3	Axisymmetric	70	4.60
ClsoT3	0.79	9.30	14.6	Axisymmetric	70	6.99
ClsoT4	0.51	6.04	8.7	Axisymmetric	70	4.51
ClsoT5	0.96	11.34	20.1	Axisymmetric	70	8.50
ClsoT6	0.77	9.06	13.4	Axisymmetric	70	6.81
ClsoT7	0.47	5.53	8.3	Axisymmetric	70	4.16
ClsoT8	1.07	12.56	26.9	Axisymmetric	70	9.47
ClsoT9	0.85	10.04	19.3	Axisymmetric	70	7.52
ClsoT10	0.64	7.52	12.5	Axisymmetric	70	5.66
CsT1	1.32	15.57	11.3	Axisymmetric	70	11.68
CsT2	0.83	9.72	3.1	Axisymmetric	70	7.35
CsT3	1.31	15.40	12.6	Axisymmetric	70	11.59
CsT4	0.97	11.44	6.4	Axisymmetric	70	8.58
CsT5	1.26	14.88	18.1	Axisymmetric	70	11.15
CsT6	1.06	12.53	11	Axisymmetric	70	9.38
CsT7	0.69	8.14	5.5	Axisymmetric	70	6.11
CsT8	1.29	15.19	22.3	Axisymmetric	70	11.42
CsT9	1.11	13.02	15	Axisymmetric	70	9.82
CsT10	0.80	9.41	8.2	Axisymmetric	70	7.08
SIsoT1	1.42	16.73	9.5	Axisymmetric	70	12.57
SIsoT2	1.19	13.97	3.3	Axisymmetric	70	10.53
SIsoT3	1.34	15.81	11.8	Axisymmetric	70	11.86
SIsoT4	1.21	14.23	7.2	Axisymmetric	70	10.71
SIsoT5	1.36	15.99	17.4	Axisymmetric	70	12.04
SIsoT6	1.20	14.06	11.5	Axisymmetric	70	10.62
SIsoT7	0.92	10.86	5.3	Axisymmetric	70	8.14
SIsoT8	1.42	16.76	22.3	Axisymmetric	70	12.57
SIsoT9	1.25	14.67	15.5	Axisymmetric	70	11.06
SIsoT10	1.13	13.32	9.9	Axisymmetric	70	10.00
CsC1	1.27	14.95	10.9	Axisymmetric	70	11.24
CsC2	0.65	7.78	4.6	Axisymmetric	70	5.75
CsC3	1.07	12.61	14.1	Axisymmetric	70	9.47
CsC4	0.78	9.13	8	Axisymmetric	70	6.9
CsC5	1.05	12.35	17.8	Axisymmetric	70	9.29
CsC6	0.84	9.87	13	Axisymmetric	70	7.43
CsC7	0.53	6.26	6.9	Axisymmetric	70	4.69
CsC8	1.13	13.33	23.3	Axisymmetric	70	10
CsC9	0.94	11.03	17.7	Axisymmetric	70	8.32
CsC10	0.65	7.64	10.8	Axisymmetric	70	5.75

**Figure 10.** Sample placement and collapse between the jaws of the Santam machine.

produced for the experimental tests. The reason was, this specific sample was hard to produce because of the relatively small corrugation size. For increasing precision and production of samples with a precise corrugation geometry that exactly resembles the simulation sample, we chose to produce the SIsoT4 sample that has a bigger corrugation

**Figure 11.** Different stages of SIsoT4 sample collapse; (a) 0% collapse, (b) 20% collapse, (c) 50% collapse.

geometry. This SIsoT4 sample is produced as the representative of the SIsoT corrugation type. It should be mentioned that the main purpose of experimental tests was to validate our numerical simulation results. Since for this validating purpose, we already compared SIsoT4 experimental and simulation results with each other in Figure 13(b), we can be assured the simulation results would be accurate for all other SIsoT samples as well. So, we do not have any experimental results for the SIsoT1 sample and just the simulation result for this sample is illustrated in Figure 15.

As can be seen in Figure 15, among all of the samples with different corrugation types, IT, SIsoT, CsT, CsC, and ClsoT samples have a higher amount of energy absorption,

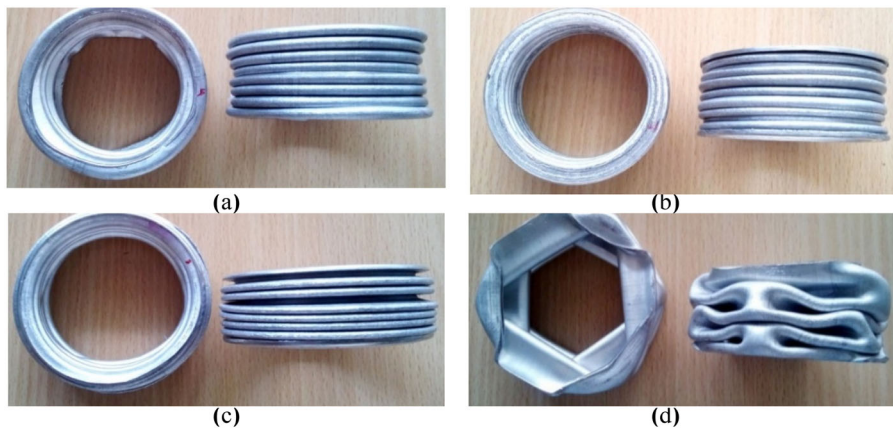


Figure 12. Different samples after collapse; (a) CsC1, (b) ClsoT1, (c) SlsoT4, (d) IT.

Table 3. Averaged collapse results of the experimental samples.

Samples name	Absorbed energy (kJ)	Average force (kN)	Maximum initial force (kN)	Collapse style	Crushing length (%)	Specific energy (kJ/kg)
IT	1.5446	18.2	39.2	Diamond	70	13.67
CsT1	1.2771	14.7	9.6	Axisymmetric	70	11.29
CsC1	1.2422	14.6	8.7	Axisymmetric	70	10.98
ClsoT6	0.7309	8.7	13.1	Axisymmetric	70	6.46
ClsoT1	1.0225	12.1	11.9	Axisymmetric	70	9.05
SlsoT4	1.1778	13.8	6.5	Axisymmetric	70	10.41

Table 4. Difference between the numerical simulation and experiment results.

Sample names	Difference %			
	Absorbed energy	Specific energy	Average force	Maximum initial force
IT	4.09	4.1	3.96	-1.53
CsT1	3.36	3.45	3.92	17.71
CsC1	2.24	2.37	2.4	25.28
ClsoT6	5.35	5.42	4.14	2.29
ClsoT1	0.73	0.77	0.33	0.84
SlsoT4	2.73	2.88	3.12	10.77

respectively. Actually, SlsoT, CsT, CsC, and ClsoT samples, approximately absorbed 88%, 82%, 79%, and 64% of the energy absorption capacity of an intact tube, respectively. Since the initial lengths of all the samples are the same and there is no change in their mass during production, so the mass of all the samples is equal; therefore, the specific energy of all of them is proportional to their absorbed energy. So, similar to the absorbed energy, IT, SlsoT, CsT, CsC, and ClsoT samples have the highest amount of specific energy, respectively. Also, the same sequence of IT, SlsoT, CsT, CsC, and ClsoT samples, respectively, have a higher amount of average collapse force as well.

So, it can be concluded that applying corrugations on an intact tube will decrease the amount of its energy absorption, specific energy, and average collapse force. Among different types of corrugations, singly isosceles triangular, continual scalene triangular, continual semi-circular, and continual isosceles triangular corrugations have a higher amount of energy absorption, specific energy, and average collapse force, respectively.

As shown in Figure 15, the amount of maximum initial force will decrease drastically by applying any corrugation. It should be mentioned that all of the samples with corrugations have approximately the same amount of maximum

initial force. So, it can be concluded that the maximum initial force is not much sensitive to the corrugation type.

The two most important characteristics of an energy absorber (bumper) are the amount of energy it absorbs and the amount of maximum initial force. A bumper that has the highest amount of energy absorption while having the lowest amount of maximum initial force is the optimum one. Therefore, among all of the samples with different corrugation types, sample SlsoT would be the most desirable one.

Also, it should be mentioned, from the force-displacement diagrams in Figure 13, it is clear that the energy absorbers experience different forces during the collapse, depending on the type of corrugation. For example, the process of changing the collapse force in the SlsoT sample increases progressively with continuing the loading, large fluctuations occur in the IT sample, and in the ClsoT model, the collapse force is more uniform and it is relatively constant during loading. Therefore, by changing the geometry of the corrugations, the force-displacement diagram pattern can be controlled as well.

4.2. Effect of the amplitude and wavelength of the corrugations

In this section, the effect of the amplitude and wavelength of the corrugations on the energy absorption characteristics are evaluated separately. For this purpose, the amount of absorbed energy, specific energy, average collapse force, and maximum initial force for each simulated sample is illustrated in a line chart (Figure 16) to better understand the trend of the results.

As shown in Figure 16, by keeping wavelength constant and increasing the amplitude of the corrugations; Case numbers 1–2, 3–4, 5–6–7, and 8–9–10 (please see Table 1. In this table, each column has the same corrugation amplitude

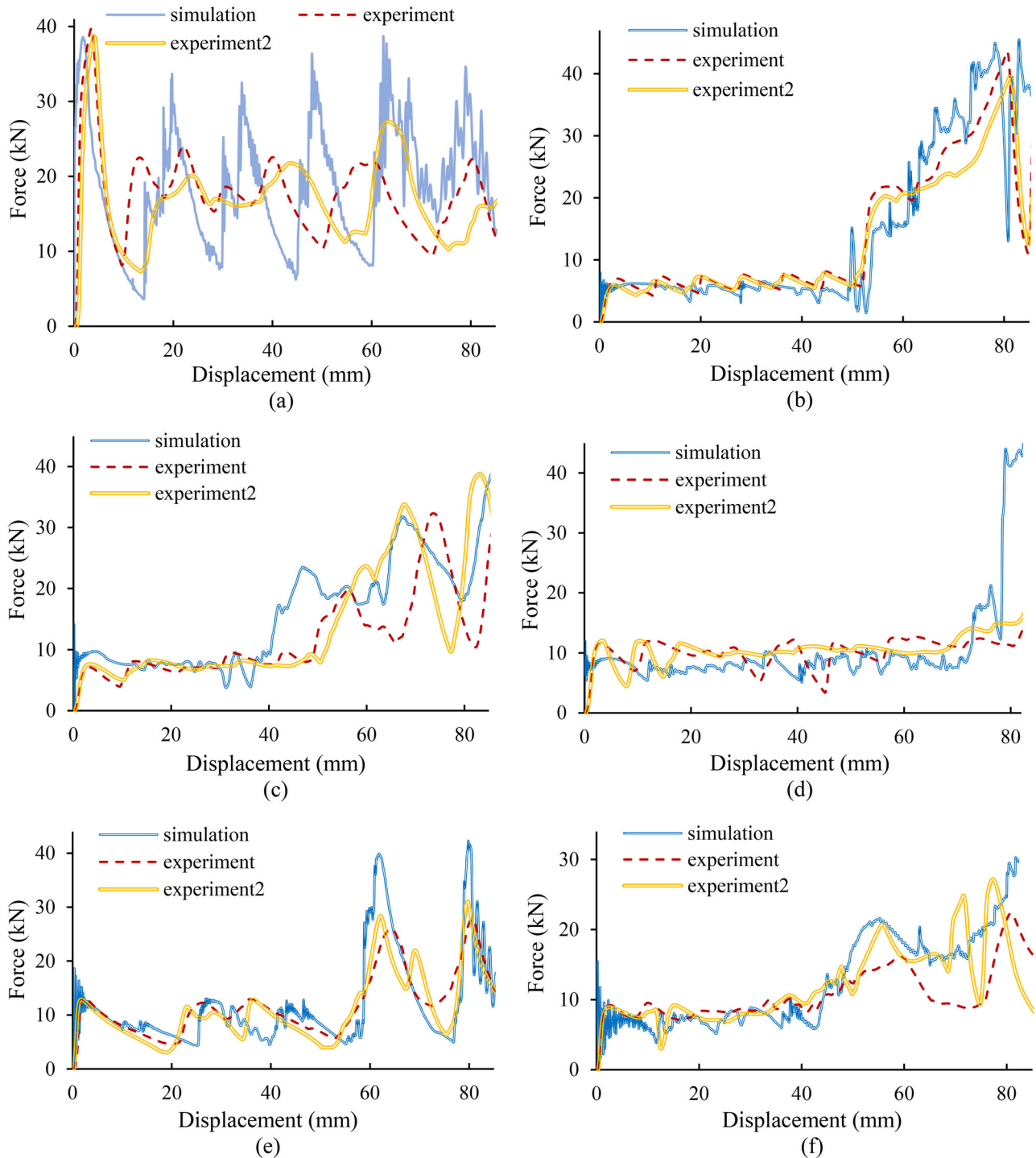


Figure 13. Comparison of force–displacement diagrams obtained from experiments and simulations; (a) IT, (b) SIsoT4, (c) CsC1, (d) ClsoT1, (e) ClsoT6, (f) CsT1.

and each row has the same wavelength.), absorbed energy, specific energy, average collapse force, and maximum initial force will decrease.

Also, by keeping the amplitude constant and increasing the wavelength; Case numbers 1–3–5–8, 2–4–6–9, and 7–10 (see Table 1), absorbed energy, specific energy, and average collapse force will be approximately constant with a slight increase. Also, the amount of the maximum initial force will increase more sharply. This is due to the smaller number of plastic hinges formed over the larger wavelengths, which leads to fewer but more intense fluctuations in the force–displacement

diagram. Finally, although the maximum initial force has grown significantly, the absorbed energy, specific energy, and average force have increased slightly.

So, for reaching the most desirable sample, we should have a tradeoff evaluation between the amount of energy absorption we need and the amount of maximum initial force that is suitable for our usage conditions. For a better understanding of obtained results and the reasons behind them, a summary of analytical analyses that existed for various corrugation geometries is elaborated in the next section. A qualitative comparison between our simulation and

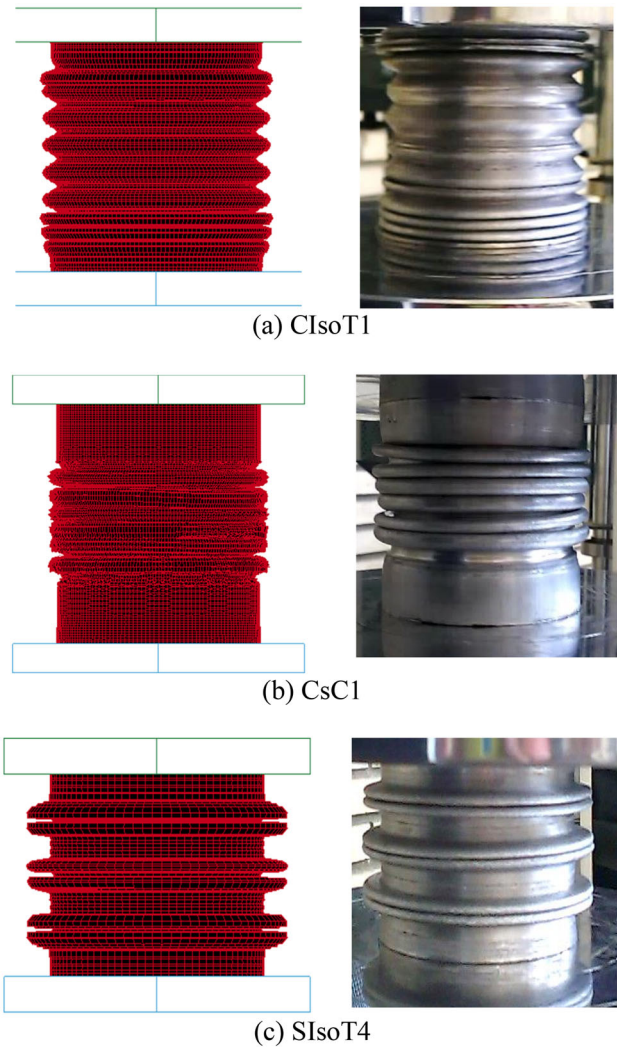


Figure 14. Comparison of several samples after 50% collapsing (Right: Experiment, left: simulation); (a) ClsoT1, (b) CsC1, (c) SIsoT4.

experimental results and the results predicted by analytical approaches are mentioned as well.

4.3. Theoretical analysis

In this section, a summary of analytical studies carried out on different corrugation geometries in cylindrical thin-walled tubes will be mentioned and their mathematical predictions will be compared with our obtained results.

There are several theoretical studies for analyzing the crushing of corrugated tubes under a quasi-static load based on specific corrugation geometries. A comprehensive review of these theoretical studies can be found in [37]. Based on the plastic deformation hypothesis that had previously been put out by Alexander [38], Abramowicz and John [39, 40], and Wierzbicki *et al.* [41], all of the mathematical models were developed. They believed that the membrane-stretching energies and plastic hinge bending would be responsible for dissipating the external energy. So, based on different collapse configurations of the tubes with different corrugation geometries, they derived an analytical formula to predict the crushing mechanism.

For example, for sinusoidal corrugation tubes, there are three different analytical studies. Hao *et al.* [42], Chen [43], and Eyvazian *et al.* [44] each carried out different mathematical approaches for reaching a formula for the mean crushing force. Also, for conical corrugation tubes (CCT) mimicking coconut tree configuration, Ha *et al.* [27] presented an analytical formula in their study for predicting the mean crushing force. Hao *et al.* and Ha *et al.* formulas are mentioned in Eqs. (3) and (4) as the representative for the sinusoidal and conical corrugations, respectively. The collapse configurations considered in their studies are shown in Figure 17 as well.

$$\begin{aligned} \text{Hao } et \text{ al. [42] formula (sinusoidal corrugation): } & \frac{P_m}{M_0} \\ &= \frac{4\pi}{\eta} \sqrt{\frac{D[\pi - 2\arcsin(2n)](1 - 2n)}{t}} \end{aligned} \quad (3)$$

$$\begin{aligned} \text{SanHa } et \text{ al. [27] formula (conical corrugation): } & \frac{P_m}{M_0} \\ &= \frac{4\pi^{3/2}}{\eta} \sqrt{\frac{D}{t}} + \frac{\pi(\sin\theta + \cos\theta)}{\eta} \end{aligned} \quad (4)$$

In the above equations and figure, P_m is the mean crushing force, $M_0 = 1/4\sigma_0 t^2$ in which σ_0 and t are the flow stress of the material and thickness of the tube, respectively, η is the effective crush distance factor. Wierzbicki and Abramowicz [1, 45] discovered that the effective crush distance in axial crushing response is around 0.70 to 0.75 of the wavelength due to the strain hardening effect, and D is the tube diameter. For the sinusoidal corrugation (Eq. 3), n is the amplitude factor in which $a = nl$. a and l are the amplitude and half arc length of a sinusoidal cycle, respectively, shown in Figure 17(a). For the conical corrugation (Eq. 4), θ is the tapered angle shown in Figure 17(f).

For evaluating the energy absorption performance of tubes with sinusoidal and conical corrugations, the theoretical mean crushing forces of them are compared with each other. In Eq. (3), since $n > 0$, the term $[\pi - 2\arcsin(2n)](1 - 2n)$ is less than π . Therefore:

$$\left(\frac{P_m}{M_0}\right)_{\text{Sinusoidal}} < \frac{4\pi^{3/2}}{\eta} \sqrt{\frac{D}{t}} \quad (5)$$

And in Eq. (4), Since $0 \leq \theta < \pi/2$, thus, $\sin \theta \geq 0$ & $\cos \theta < 1$. As the result:

$$\left(\frac{P_m}{M_0}\right)_{\text{Conical}} > \frac{4\pi^{3/2}}{\eta} \sqrt{\frac{D}{t}} \quad (6)$$

By comparing Eq. (5) with Eq. (6), it can be concluded that the mean force in conical corrugation tubes would be higher than that of sinusoidal corrugation tubes.

Although the corrugation geometries considered in our study don't fit exactly with the two previously mentioned geometries. But our CsC (continual semi-circular corrugation) is very similar to the sinusoidal corrugation mentioned in Hao *et al.* study and our CsT (continual scalene

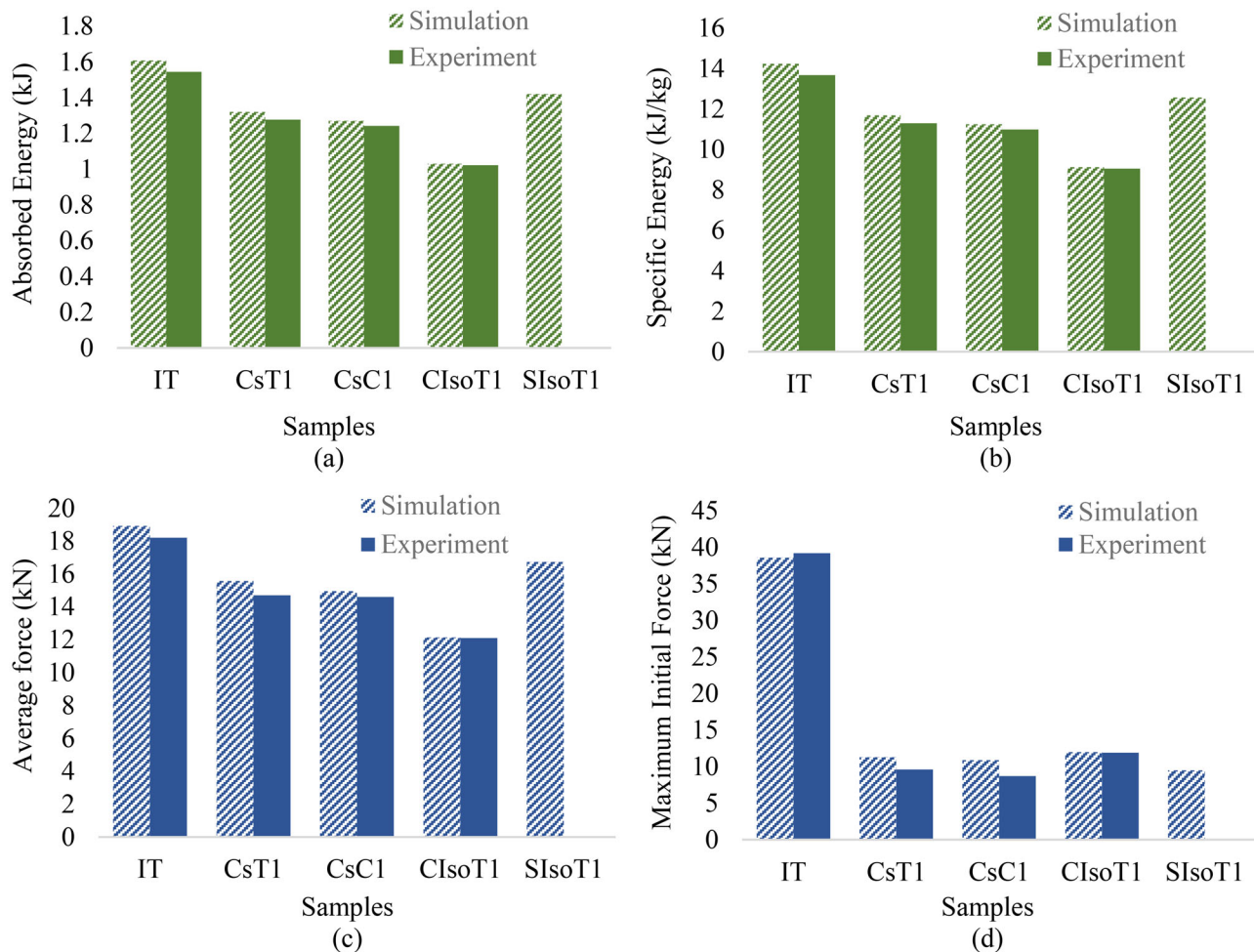


Figure 15. The effect of the corrugation's geometry on the collapse characteristics of the absorbers; (a) absorbed energy, (b) specific energy, (c) average collapse force, (d) maximum initial force.

triangular corrugation) is very analogous to conical corrugation considered by Ha *et al.* So, it can be assumed that the collapse configuration of our samples should be almost the same as theirs. Therefore, their derived theoretical equations should work for our CsC and CsT geometries as well. As you can see in Figure 16(c), for samples with equal state numbers (corrugations with the same wavelength and amplitude), the average crushing force of CsT (analogous to conical corrugation) is always higher than CsC (analogous to sinusoidal corrugation). These obtained results from our simulation and experiments agree exactly with the predictions carried out by the analytical formulas.

Furthermore, based on Hao *et al.*'s [42] theoretical model and their simplifying considerations, such as treating the distance between two stationary hinges as a straight line rather than a curve (shown in Figures 3 and 4 of their paper), we can conclude that the collapse configuration of our CIsoT sample should be very similar to the CsC one. So, based on their theoretical model the results obtained for the average crushing force for CIsoT and CsC samples should be pretty much equal. As shown in Figure 16(c), for samples with state numbers higher than 5, the average crushing force of CIsoT and CsC samples are almost the same which agrees with our previous statement. The difference between the average crushing

force in the CIsoT and CsC samples will only increase for small state numbers, which correspond to smaller wavelengths (higher number of corrugations), which is logical given that the number of corrugations will increase the cumulative effect of this difference between corrugation geometries.

Also, by looking at our SIsoT geometry, you can see the corrugations are kind of far from each other in comparison to other corrugation geometries considered. This suggests that the collapse configuration of the SIsoT samples should be the most comparable to that of the IT (intact tube) sample, and thus the findings obtained for the SIsoT and IT samples should be the most similar among other samples. By looking at Figure 15(c), you can see that the average crushing force of SIsoT1 and IT samples are pretty much the same which agrees with the assumption about the collapse configurations of these samples mentioned previously.

According to the findings, theoretical formulae can be highly beneficial for forecasting the energy absorption performance of thin-walled tubes with various forms of corrugations. However, because each of the many corrugation geometries has its own distinct theoretical model, more research on this subject is needed to establish theoretical formulations for each individual corrugation geometry.

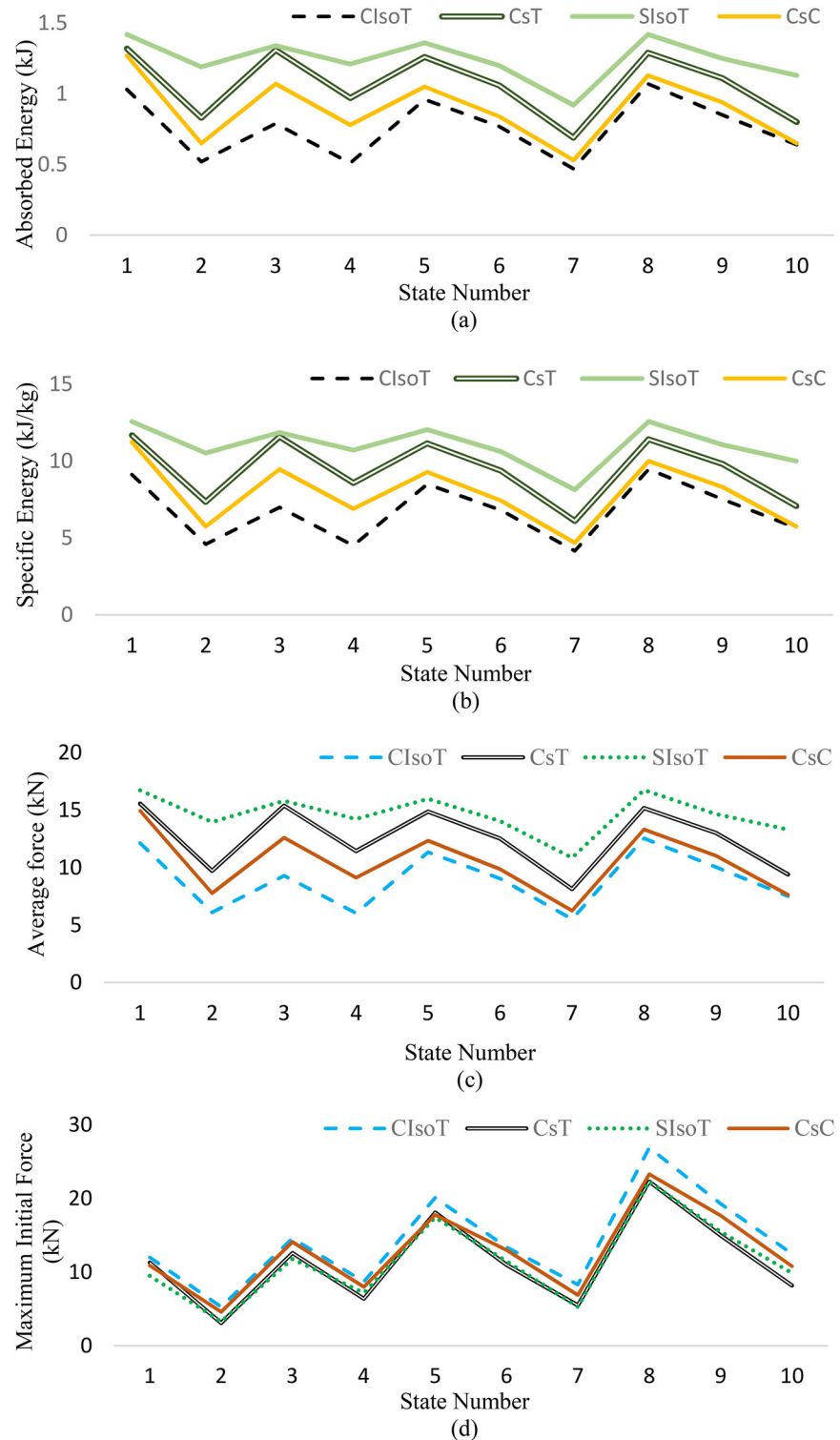


Figure 16. The effect of amplitude and wavelength of the corrugations (line chart); (a) absorbed energy, (b) specific energy, (c) average collapse force, (d) maximum initial force.

5. Conclusion

The purpose of this article is to investigate the effect of the geometry of peripheral corrugations on the mechanical behavior of cylindrical thin-walled tubes, including the method of collapsing and the amounts of absorbed energy, specific energy, average collapse force, and maximum initial force. For this purpose, numerical simulations and experimental tests were performed. A comparison of our acquired

results with theoretical research was also undertaken to understand the logic of our results from a theoretical standpoint. According to the evaluations conducted in the results and discussion section, the main conclusions of this research are as follows:

1. Applying corrugations with different geometry types will decrease the amount of energy absorption, specific

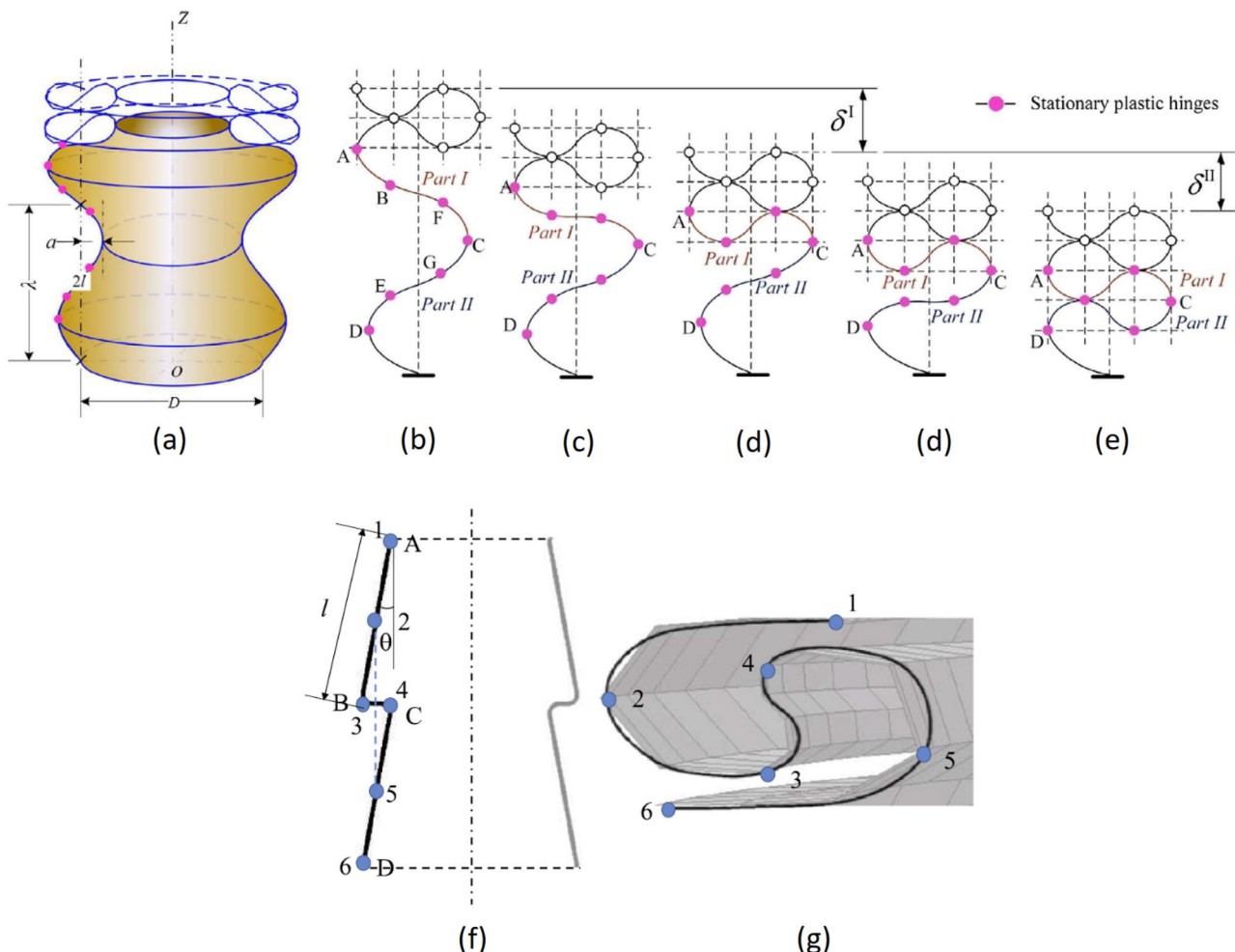


Figure 17. Schematic of collapse configuration of tubes with sinusoidal and conical corrugations under a quasi-static load: (a)–(e) Sinusoidal corrugated tube along with its complete fold (consisting of part I and part II) [42]; (f, g) Conical corrugated tube initial and deformed conditions [27].

- energy, and average collapse force in thin-walled cylindrical tubes.
2. SIsoT, CsT, CsC, and CIsoT samples, approximately absorb 88%, 82%, 79%, and 64% of the energy absorption capacity of an intact tube, respectively.
 3. In general, the formation of peripheral corrugations severely reduces the initial maximum force in cylindrical tubes. SIsoT, CsT, CsC, and CIsoT samples, approximately have 25%, 29%, 28%, and 31% of the maximum initial force of an intact tube.
 4. Singly isosceles triangular corrugation due to having the lowest amount of maximum initial force and relatively the highest amount of energy absorption among all of the samples with different corrugation types would be chosen as the most desirable corrugation type.
 5. By changing the geometry of the corrugations, the force–displacement diagram pattern can be controlled for reaching a more uniform force–displacement diagram with less severe fluctuations.
 6. By keeping the wavelength constant and increasing the amplitude of the corrugations, absorbed energy, specific energy, average collapse force, and maximum initial force will decrease.

7. By keeping the amplitude constant and increasing the wavelength, absorbed energy, specific energy, and average collapse force will slightly increase (approximately stay constant) but the maximum initial force will increase more sharply.
8. The experimental and simulation results obtained are in good agreement with theoretical formulas and such a trend in obtained results can be predicted effectively by previous theoretical studies in this field.

References

- [1] T. Wierzbicki and W. Abramowicz, On the Crushing Mechanics of Thin-Walled Structures, ASME. J. Appl. Mech., vol. 50, no. 4a, pp. 727–734, 1983. <https://doi.org/10.1115/1.3167137>.
- [2] W. Abramowicz, The effective crushing distance in axially compressed thin-walled metal columns, Int. J. Impact Eng., vol. 1, no. 3, pp. 309–317, 1983. DOI: [10.1016/0734-743X\(83\)90025-8](https://doi.org/10.1016/0734-743X(83)90025-8).
- [3] W. Abramowicz and N. Jones, Dynamic progressive buckling of circular and square tubes, Int. J. Impact Eng., vol. 4, no. 4, pp. 243–270, 1986. DOI: [10.1016/0734-743X\(86\)90017-5](https://doi.org/10.1016/0734-743X(86)90017-5).
- [4] W. Abramowicz and N. Jones, Dynamic axial crushing of square tubes, Int. J. Impact Eng., vol. 2, no. 2, pp. 179–208, 1984. DOI: [10.1016/0734-743X\(84\)90005-8](https://doi.org/10.1016/0734-743X(84)90005-8).
- [5] M. Langseth T. Berstad, O. Hopperstad, and A. Clausen, Energy absorption in axially loaded square thin-walled

- aluminium extrusions, WIT Trans. Built Environ., vol. 8, pp. 8, 1970. <https://www.witpress.com/elibrary/wittransactions-on-the-built-environment/8/11973>
- [6] S. Lee, C. Hahn, M. Rhee, and J.-E. Oh, Effect of triggering on the energy absorption capacity of axially compressed aluminum tubes, Mater. Des., vol. 20, no. 1, pp. 31–40, 1999. DOI: [10.1016/S0261-3069\(98\)00043-0](https://doi.org/10.1016/S0261-3069(98)00043-0).
- [7] R. Kalhor, Energy Absorption of Metal-FRP Hybrid Square Tubes, Virginia Tech Electronic Theses and Dissertations, Doctoral Dissertations, 2017. <https://vtworks.lib.vt.edu/handle/10919/74960>
- [8] S.R. Reid, T. Reddy, and M. Gray, Static and dynamic axial crushing of foam-filled sheet metal tubes, Int. J. Mech. Sci., vol. 28, no. 5, pp. 295–322, 1986. DOI: [10.1016/0020-7403\(86\)90043-3](https://doi.org/10.1016/0020-7403(86)90043-3).
- [9] T. Reddy and R. Wall, Axial compression of foam-filled thin-walled circular tubes, Int. J. Impact Eng., vol. 7, no. 2, pp. 151–166, 1988. DOI: [10.1016/0734-743X\(88\)90023-1](https://doi.org/10.1016/0734-743X(88)90023-1).
- [10] A.A. Nia and J.H. Hamedani, Comparative analysis of energy absorption and deformations of thin walled tubes with various section geometries, Thin. Walled Struct., vol. 48, no. 12, pp. 946–954, 2010.
- [11] J. Bi, H. Fang, Q. Wang, and X. Ren, Modeling and optimization of foam-filled thin-walled columns for crashworthiness designs, Finite Elem. Anal. Des., vol. 46, no. 9, pp. 698–709, 2010. DOI: [10.1016/j.finel.2010.03.008](https://doi.org/10.1016/j.finel.2010.03.008).
- [12] H. Luo, Y. Yan, X. Meng, and C. Jin, Progressive failure analysis and energy-absorbing experiment of composite tubes under axial dynamic impact, Compos. B: Eng., vol. 87, pp. 1–11, 2016. DOI: [10.1016/j.compositesb.2015.10.016](https://doi.org/10.1016/j.compositesb.2015.10.016).
- [13] A.A. Nia and S. Chahardoli, Optimizing the layout of nested three-tube structures in quasi-static axial collapse, Thin. Walled Struct., vol. 107, pp. 169–181, 2016. DOI: [10.1016/j.tws.2016.06.010](https://doi.org/10.1016/j.tws.2016.06.010).
- [14] C. Yang, Y. Tian, P. Xu, S. Yao, Z. Li, and M.S. Alqahtani, Crashworthiness optimization of a multicellular thin-walled tube with triangular cells, Mech. Adv. Mater. Struct., vol. 29, no. 28, pp. 7277–7293, 2022. DOI: [10.1080/15376494.2021.1995548](https://doi.org/10.1080/15376494.2021.1995548).
- [15] L. Zhang, Y. Zhong, W. Tan, C. Gong, Y. Hu, and Z. Bai, Crushing characteristics of bionic thin-walled tubes inspired by bamboo and beetle forewing, Mech. Adv. Mater. Struct., vol. 29, no. 14, pp. 2024–2039, 2022. DOI: [10.1080/15376494.2020.1849880](https://doi.org/10.1080/15376494.2020.1849880).
- [16] C. Zhang, Y. Sun, J.L. Curiel-Sosa, and D. Zhang, Numerical analysis on axial crushing damage of aluminum/CFRP hybrid thin-walled tubes, Mech. Adv. Mater. Struct., pp. 1–11, 2023. DOI: [10.1080/15376494.2023.2213225](https://doi.org/10.1080/15376494.2023.2213225).
- [17] T. Olutola, J. Balen, V. Lotisa, A. Johnima, and I. Browndi, Sustainable decision-making for thin-walled structures: A comprehensive review, Asian J. Basic Appl. Sci., vol. 11, no. 01, pp. 399–403, 2023.
- [18] J. Ma, S. Chai, and Y. Chen, Geometric design, deformation mode, and energy absorption of patterned thin-walled structures, Mech. Mater., vol. 168, pp. 104269, 2022. DOI: [10.1016/j.mechmat.2022.104269](https://doi.org/10.1016/j.mechmat.2022.104269).
- [19] G. Daneshi and S. Hosseiniipour, Grooves effect on crashworthiness characteristics of thin-walled tubes under axial compression, Mater. Des., vol. 23, no. 7, pp. 611–617, 2002. DOI: [10.1016/S0261-3069\(02\)00052-3](https://doi.org/10.1016/S0261-3069(02)00052-3).
- [20] M. Rezvani and M. Damghani Nouri, Analytical model for energy absorption and plastic collapse of thin-walled grooved frusta tubes, Mech. Adv. Mater. Struct., vol. 22, no. 5, pp. 338–348, 2015. DOI: [10.1080/15376494.2012.736054](https://doi.org/10.1080/15376494.2012.736054).
- [21] A. Asanjarani, A. Mahdian, and S. Dibajian, Comparative analysis of energy absorption behavior of tapered and grooved thin-walled tubes with the various geometry of the cross section, Mech. Adv. Mater. Struct., vol. 27, no. 8, pp. 633–644, 2020. DOI: [10.1080/15376494.2018.1488311](https://doi.org/10.1080/15376494.2018.1488311).
- [22] S. Xie, P. Chen, N. Wang, J. Wang, and X. Du, Crashworthiness study of circular tubes subjected to radial extrusion under quasi-static loading, Int. J. Mech. Sci., vol. 192, pp. 106128, 2021. DOI: [10.1016/j.ijmecsci.2020.106128](https://doi.org/10.1016/j.ijmecsci.2020.106128).
- [23] A. Eyyazian, I. Akbarzadeh, and M. Shakeri, Experimental study of corrugated tubes under lateral loading, Proc. Inst. Mech. Eng. L: J. Mater.: Des. Appl., vol. 226, no. 2, pp. 109–118, 2012. DOI: [10.1177/1464420712437307](https://doi.org/10.1177/1464420712437307).
- [24] A. Eyyazian M.K. Habibi, A.M. Hamouda, and R. Hedayati, Axial crushing behavior and energy absorption efficiency of corrugated tubes, Mater. Des. (1980–2015), vol. 54, pp. 1028–1038, 2014. DOI: [10.1016/j.matdes.2013.09.031](https://doi.org/10.1016/j.matdes.2013.09.031).
- [25] S. Rawat, A. Narayanan, T. Nagendiran, and A.K. Upadhyay, Collapse behavior and energy absorption in elliptical tubes with functionally graded corrugations, Proc. Eng., vol. 173, pp. 1374–1381, 2017. DOI: [10.1016/j.proeng.2016.12.194](https://doi.org/10.1016/j.proeng.2016.12.194).
- [26] M. Abolfathi and A.A. Nia, Optimization of energy absorption properties of thin-walled tubes with combined deformation of folding and circumferential expansion under axial load, Thin. Walled Struct., vol. 130, pp. 57–70, 2018. DOI: [10.1016/j.tws.2018.05.011](https://doi.org/10.1016/j.tws.2018.05.011).
- [27] N. San Ha, G. Lu, and X. Xiang, High energy absorption efficiency of thin-walled conical corrugation tubes mimicking coconut tree configuration, Int. J. Mech. Sci., vol. 148, pp. 409–421, 2018. DOI: [10.1016/j.ijmecsci.2018.08.041](https://doi.org/10.1016/j.ijmecsci.2018.08.041).
- [28] A. Sadighi, A. Eyyazian, M. Asgari, and A.M. Hamouda, A novel axially half corrugated thin-walled tube for energy absorption under axial loading, Thin. Walled Struct., vol. 145, pp. 106418, 2019. DOI: [10.1016/j.tws.2019.106418](https://doi.org/10.1016/j.tws.2019.106418).
- [29] A. Eyyazian, S. Najafian, H. Mozafari, and A. Praveen Kumar, Crashworthiness Analysis of a Novel Aluminum Bi-tubular Corrugated Tube—Experimental Study. In: Vijay Sekar, K., Gupta, M., Arockiarajan, A. (eds) Advances in Manufacturing Processes. Lecture Notes in Mechanical Engineering. Springer, Singapore. https://doi.org/10.1007/978-981-13-1724-8_55
- [30] W. Ma, Z. Li, and S. Xie, Crashworthiness analysis of thin-walled bio-inspired multi-cell corrugated tubes under quasi-static axial loading, Eng. Struct., vol. 204, pp. 110069, 2020. DOI: [10.1016/j.engstruct.2019.110069](https://doi.org/10.1016/j.engstruct.2019.110069).
- [31] Z. Li, M. Wen, X. Ping, and Y. Shuguang, Crashworthiness of multi-cell circumferentially corrugated square tubes with cosine and triangular configurations, Int. J. Mech. Sci., vol. 165, pp. 105205, 2020. DOI: [10.1016/j.ijmecsci.2019.105205](https://doi.org/10.1016/j.ijmecsci.2019.105205).
- [32] Z. Li, W. Ma, S. Yao, and P. Xu, Crashworthiness performance of corrugation-reinforced multicell tubular structures, Int. J. Mech. Sci., vol. 190, pp. 106038, 2021. DOI: [10.1016/j.ijmecsci.2020.106038](https://doi.org/10.1016/j.ijmecsci.2020.106038).
- [33] M. Yang, B. Han, P. Su, Q. Zhang, Q.C. Zhang, Z. Zhao, C. Ni, and T.J. Lu, Crashworthiness of hierarchical truncated conical shells with corrugated cores, Int. J. Mech. Sci., vol. 193, pp. 106171, 2021. DOI: [10.1016/j.ijmecsci.2020.106171](https://doi.org/10.1016/j.ijmecsci.2020.106171).
- [34] Z. Li, W. Ma, H. Zhu, G. Deng, L. Hou, P. Xu, and S. Yao, Energy absorption prediction and optimization of corrugation-reinforced multicell square tubes based on machine learning, Mech. Adv. Mater. Struct., vol. 29, no. 26, pp. 5511–5529, 2022. DOI: [10.1080/15376494.2021.1958032](https://doi.org/10.1080/15376494.2021.1958032).
- [35] K. Andrews, G. England, and E. Ghani, Classification of the axial collapse of cylindrical tubes under quasi-static loading, Int. J. Mech. Sci., vol. 25, no. 9–10, pp. 687–696, 1983. DOI: [10.1016/0020-7403\(83\)90076-0](https://doi.org/10.1016/0020-7403(83)90076-0).
- [36] ASTM E8/E8M-16a1, Standard Test Methods for Tension Testing of Metallic Materials, ASTM International, West Conshohocken, PA, 2016. www.astm.org.
- [37] N. San Ha and G. Lu, Thin-walled corrugated structures: A review of crashworthiness designs and energy absorption characteristics, Thin. Walled Struct., vol. 157, pp. 106995, 2020. DOI: [10.1016/j.tws.2020.106995](https://doi.org/10.1016/j.tws.2020.106995).
- [38] J.M. Alexander, An approximate analysis of the collapse of thin cylindrical shells under axial loading, Q. J. Mech. Appl. Math., vol. 13, no. 1, pp. 10–15, 1960. DOI: [10.1093/qjmam/13.1.10](https://doi.org/10.1093/qjmam/13.1.10).
- [39] W. Abramowicz and N. Jones, Dynamic axial crushing of circular tubes, Int. J. Impact Eng., vol. 2, no. 3, pp. 263–281, 1984. DOI: [10.1016/0734-743X\(84\)90010-1](https://doi.org/10.1016/0734-743X(84)90010-1).

- [40] W. Abramowicz and N. Jones, Dynamic progressive buckling of circular and square tubes, *Int. J. Impact Eng.*, vol. 2, no. 2, pp. 179–208, 1984. DOI: [10.1016/0734-743X\(84\)90005-8](https://doi.org/10.1016/0734-743X(84)90005-8).
- [41] T. Wierzbicki, S.U. Bhat, W. Abramowicz, and D. Brodkin, Alexander revisited—A two folding elements model of progressive crushing of tubes, *Int. J. Solids Struct.*, vol. 29, no. 24, pp. 3269–3288, 1992. DOI: [10.1016/0020-7683\(92\)90040-Z](https://doi.org/10.1016/0020-7683(92)90040-Z).
- [42] W. Hao, J. Xie, and F. Wang, Theoretical prediction of the progressive buckling and energy absorption of the sinusoidal corrugated tube subjected to axial crushing, *Comput. Struct.*, vol. 191, pp. 12–21, 2017. DOI: [10.1016/j.compstruc.2017.05.001](https://doi.org/10.1016/j.compstruc.2017.05.001).
- [43] D.-H. Chen, *Crush Mechanics of Thin-Walled Tubes*, Book *Crush Mechanics of Thin-Walled Tubes*, CRC Press, 2015. <https://www.taylorfrancis.com/books/mono/10.1201/9781351228688/crush-mechanics-thin-walled-tubesdai-heng-chen>
- [44] A. Eyzazian, T. Tran, and A.M. Hamouda, Experimental and theoretical studies on axially crushed corrugated metal tubes, *Int. J. Non. Linear Mech.*, vol. 101, pp. 86–94, 2018. DOI: [10.1016/j.ijnonlinmec.2018.02.009](https://doi.org/10.1016/j.ijnonlinmec.2018.02.009).
- [45] W. Abramowicz and T. Wierzbicki, Axial Crushing of Multicorner Sheet Metal Columns, *ASME. J. Appl. Mech.* vol. 56, no. 1, pp. 113–120. 1989. <https://doi.org/10.1115/1.3176030>.